

A nanoengine governor based on the end interfacial effect

This content has been downloaded from IOPscience. Please scroll down to see the full text.

2016 *Nanotechnology* 27 495704

(<http://iopscience.iop.org/0957-4484/27/49/495704>)

[View the table of contents for this issue](#), or go to the [journal homepage](#) for more

Download details:

IP Address: 131.215.225.9

This content was downloaded on 30/11/2016 at 19:57

Please note that [terms and conditions apply](#).

You may also be interested in:

[Sudden stoppage of rotor in a thermally driven rotary motor made from double-walled carbon nanotubes](#)

K Cai, J Z Yu, H Yin et al.

[Quantitative control of a rotary carbon nanotube motor under temperature stimulus](#)

Kun Cai, Jing Wan, Qing H Qin et al.

[Gradientless temperature-driven rotating motor from a double-walled carbon nanotube](#)

K Cai, Y Li, Q H Qin et al.

[Controllable nanoscale rotating actuator system based on carbon nanotube and graphene](#)

Jianzhang Huang and Qiang Han

[Oscillators based on double-walled armchair@zigzag carbon nanotubes containing inner tubes with different helical rises](#)

Yong-Hui Zeng, Wu-Gui Jiang and Qing H Qin

[Energy dissipation of high-speed nanobearings from double-walled carbon nanotubes](#)

Chunzhang Zhu, Wanlin Guo and Tongxi Yu

[Sustaining GHz oscillation of carbon nanotube based oscillators via a MHz frequency excitation](#)

Benyamin Motevali, Neda Taherifar and Jefferson Zhe Liu

[Low frequency vibration of multiwall carbon nanotubes with heterogeneous boundaries](#)

R Chowdhury, C Y Wang and S Adhikari

[Investigation of the effects of commensurability on friction between concentric carbon nanotubes](#)

Chunzhang Zhu, Prathamesh M Shenai and Yang Zhao

A nanoengine governor based on the end interfacial effect

Jiao Shi¹, Kun Cai^{1,2,3} and Qing-Hua Qin^{2,3}

¹ College of Water Resources and Architectural Engineering, Northwest A&F University, Yangling 712100, People's Republic of China

² Research School of Engineering, The Australian National University, ACT, 2601, Australia

E-mail: kuncai99@163.com and qinghua.qin@anu.edu.au

Received 1 August 2016, revised 22 September 2016

Accepted for publication 23 September 2016

Published 9 November 2016



Abstract

A conceptual design is presented for a nanoengine governor based on the end interfacial effect of two rotary nanotubes. The governor contains a thermal-driven rotary nanomotor made from double-walled carbon nanotubes (DWCNTs) and a coaxially laid out rotary nanotube near one end of the nanomotor rotor. The rotation of the rotor in the nanomotor can be controlled by two features. One is the stator (the outer tube of DWCNTs) which has some end atoms with inward radial deviation (IRD) on the stator. The other is the relative rotation of the neighboring rotary tube of the rotor. As the configuration of the stator is fixed, the end interfacial interaction between the two rotors will govern the dynamic response of the rotor in the nanomotor system. The obtained results demonstrate that the relative rotational speed between the two rotors provides friction on the rotor in the nanomotor system. In particular, higher relative rotational speed will provide lower friction on rotor 1, which is opposite to that between neighboring shells in DWCNTs.

Online supplementary data available from stacks.iop.org/NANO/27/495704/mmedia

Keywords: nanomotor, carbon nanotube, interfacial effect, molecular dynamics

(Some figures may appear in colour only in the online journal)

1. Introduction

Carbon nanotubes (CNTs) were discovered by Iijima [1] in TEM observations about a quarter of century ago. Due to their excellent electrical and mechanical properties CNTs have achieved wide application in various nanodevices such as resonators [2–5], oscillators [6–10], nanosensors [11–13] and motors/bearings [14–23]. It should be mentioned that the physical properties of these structures are significantly affected by the electron structure of honeycomb-like shells. For example, the super high modulus/strength [24, 25] within shells is caused by the strong sp^2 carbon–carbon covalent bonding, whilst the superlubrication between neighboring shells in multiwalled CNTs (MWCNTs) [26] is caused by the anti-bonding electrons. These two excellent mechanical properties demonstrate that CNTs can be used to make the components in a dynamic nanodevice with structural

robustness and lower energy dissipation. Besides the covalent bonding interaction among atoms in CNTs, the van der Waals (vdW) interaction plays a major role in their dynamic response. For example, the CNT-based gigahertz oscillator described by Zheng and Jiang [7] works under the control of vdW between tube ends and between shells; specifically, the vdW interaction between tube ends provides a potential barrier which leads to the oscillation of inner tubes in the fixed outer tubes; however, the intershell vdW interaction results in a damping state during axial oscillation. This means that the intershell vdW interaction can be considered as a kind of generalized friction, which results in phonon scattering and further generates energy dissipation (from translational kinetic energy to thermal energy).

During the last decade, intershell friction has attracted much attention from researchers [6, 7, 10, 27–31]. Zhu *et al* [29] stated that the intershell friction depends not only on the sizes of tubes but also their relative sliding speed. They found that the relative sliding between tubes was caused by the

³ Authors to whom any correspondence should be addressed.

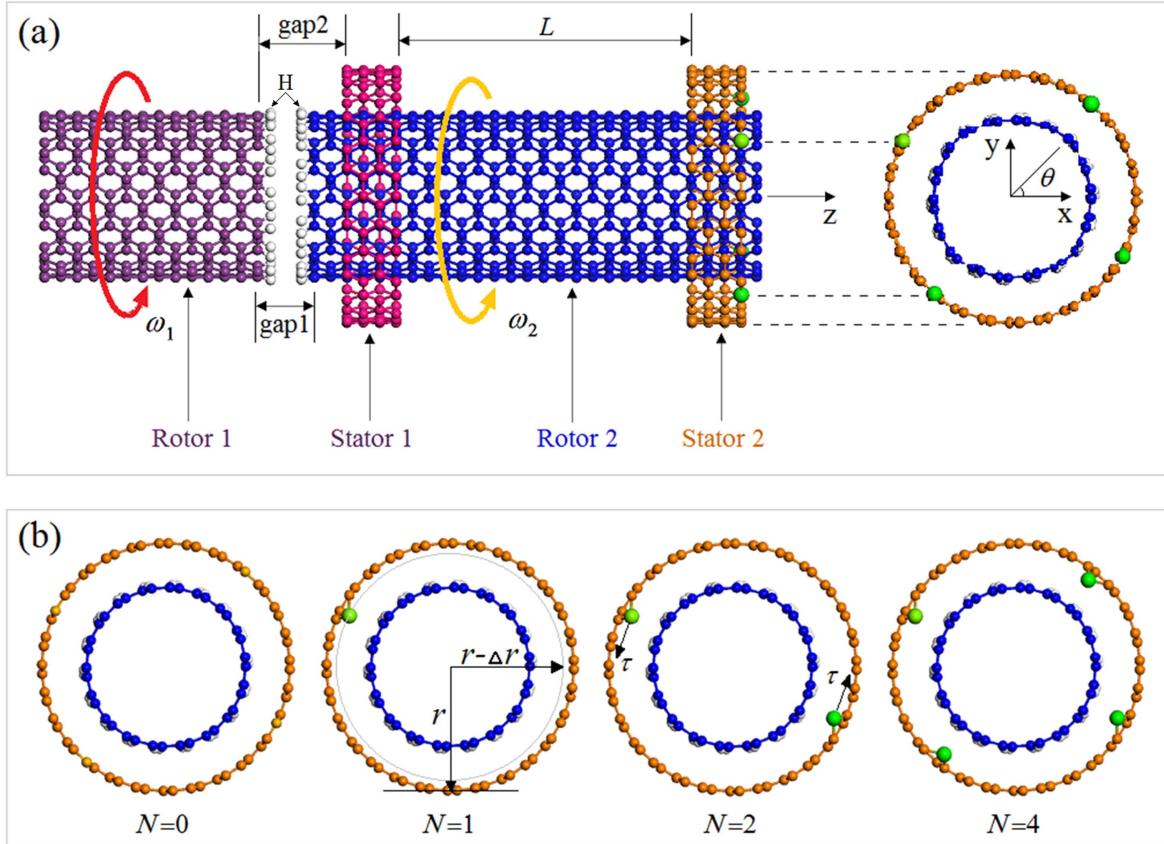


Figure 1. The geometric model of a CNT-based nanoengine governor system in Cartesian coordinate system xyz. (a) The system contains rotor 1 which has fixed rotation of ω_1 , and a thermally driven nanomotor which has two stators and a rotor (rotor 2). (b) Axial view of the system from the right end of stator 2, which has N ($N = 0, 1, 2$ or 4) end atoms with the same inward radial deviation (IRD) of $\Delta r = e \times 0.142$ nm. ‘e’ is the relative radial deviation in [0.1, 0.4]. The end atoms are called IRD atoms. The two rotors are made from the (9, 9) CNT, and the two stators from the (14, 14) tube.

rotation of the inner tube in a fixed outer tube. In such a situation, the interaction between tube ends provides resistance rather than power for the rotation of the inner tube. Guo *et al* [30] presented an explanation of the end effect, which is caused by the depth of the potential wall near the ends of the shorter tube. They found that the interaction between end atoms and inner atoms on neighboring tubes are around 20 times higher than that between inner atoms on different tubes. Cai *et al* [32] built a rotation transmission system (figure 1(a), when $N = 0$) based on the strong vdW interaction at the adjacent ends of two co-axial CNTs. Making use of the end effect, a rotary CNT can rotate the other tube with either synchronous or asynchronous rotational speeds. The transmission effect depends on such factors as the configuration of adjacent ends [33]. In the work of Cai *et al* [34], an over-speeding rotation transmission system was proposed based on the end interfacial effect.

In the studies mentioned above, the two tubes had the same rotational direction in general, namely, either clockwise or anti-clockwise along the cylindrical axis, simultaneously. And the fixed outer tube in the rotational transmission system was an ideal cylindrical shell. If the system shown in figure 1(a), has no rotor 1 and $N > 0$, the system is called a thermally driven rotary nanomotor [22], in which a number of end atoms on the stator have inward radial deviation (IRD).

The rotation of rotor 2 can be actuated if the IRD atoms are laid out in chirality. However, the system shown in figure 1(a) indicates that the rotation of rotor 2 will be governed by both rotor 1 and the two stators. In the present study, we study the end interfacial effect between two rotors by adjusting the spatial positions of the IRD atoms on stator 2. Using molecular dynamics simulations, the end interfacial effect on both the rotational direction and the speed of the inner tube is demonstrated. The results show that the system shown in figure 1(a) can be considered as a nanoengine governor.

2. Models and methodology

Figure 1 lists the initial ideal configuration of the interaction system. The major steps in our simulation are as follows. Step (1): create a physical model as shown in figure 1 with $L = 2.221$ nm, $gap 1 = 0.426$ nm and $gap 2 = 0.671$ nm, respectively. The axial linear motion of rotor 2 will be confined to keep a strong interaction between the two rotors. Step (2): reshape the positions of atoms in the system using energy minimization by the steepest descent algorithm. The tolerance of the algorithm for energy and force is set to be 10^{-8} . After minimization of potential energy, fix the degrees of freedom of all atoms on stators and some atoms on two rotors. Step

(3): put atoms in some initial velocities in a thermal bath in a canonical NVT ensemble with temperature $T = 300$ K. Step (4): after 200 ps of relaxation, let rotor 1 rotate at a constant rotational frequency, say 200 GHz, and release rotor 2 to move freely in the same canonical NVT ensemble. Step (5): run for 15 000 ps and save the data for post-processing. In our simulation, the time step for the integral of the Newton's second law of motion is 0.001 ps.

The open-source code LAMMPS [35, 36] is used for the present simulation, in which the interaction among carbon and/or hydrogen atoms is described using the AIREBO potential [37]. The potential function contains three major terms:

$$\left\{ \begin{array}{l} P = P_{\text{REBO}} + P_{\text{Tors}} + P_{\text{L-J}}, \\ P_{\text{REBO}} = \sum_i \sum_{j(j>i)} [V_{ij}^{\text{R}}(r_{ij}) - b_{ij} V_{ij}^{\text{A}}(r_{ij})], \\ P_{\text{Tors}} = \frac{1}{2} \sum_i \sum_{j(j=i)} \sum_{k(k=i,j)} \sum_{l(l=i,j,k)} w_{ij} \cdot w_{jk} \cdot w_{kl} \cdot V_{\text{Tors}}(\omega_{ijkl}), \\ P_{\text{L-J}} = \sum_i \sum_{j(j>i)} 4\varepsilon \left[\left(\frac{\sigma}{r_{ij}} \right)^{12} - \left(\frac{\sigma}{r_{ij}} \right)^6 \right], \end{array} \right. \quad (1)$$

where P_{REBO} is the second-generation REBO potential for describing short-range interaction of atoms, in which V_{ij}^{R} and V_{ij}^{A} represent repulsive and attractive pairwise potentials of atoms i and j with/without the existence of other atoms. r_{ij} is the distance between atoms i and j , and b_{ij} is the coefficient of the many-body term. P_{Tors} is a term dependent on the dihedral angle ω_{ijkl} , the bond weight w_{ij} is in [0, 1] and V_{Tors} is the dihedral-angle potential. $P_{\text{L-J}}$ is the Lennard-Jones potential [38] to describe the non-bonded intermolecular interactions, in which balance distances are $\sigma_{\text{C-C}} = 0.34$ nm, $\sigma_{\text{H-H}} = 0.265$ nm, $\sigma_{\text{C-H}} = (\sigma_{\text{C-C}} + \sigma_{\text{H-H}})/2$, respectively. Parameters $\varepsilon_{\text{C-C}} = 2.84$ meV, $\varepsilon_{\text{H-H}} = 1.5$ meV and $\varepsilon_{\text{C-H}} = 1.376$ meV. The cutoff is 1.02 nm.

The rotational frequency of rotor 2 can be calculated using the following equation, i.e.

$$\omega_2(t) = \frac{1}{2\pi} \int_{s=0}^{s=t} (M_{\text{R2}}/J_{\text{R2}}) ds, \quad (2)$$

where J_{R2} is the moment of inertia of rotor 2 along the z -axis, and can be described as

$$J_{\text{R2}} = \sum_{i=1}^{i=N_2} m_i \cdot r_i^2, \quad (3)$$

where m_i and r_i are the mass of atom i and the distance between the atom and the z -axis, respectively.

The circumferential torque moment on rotor 2 contains three items and can be expressed as

$$\begin{aligned} M_{\text{R2}} &= M_{\text{R1}} + M_{\text{IRD}} + M_{\text{Sta}} \\ &= F_{\text{R1}} \cdot r_{\text{R2}} + (F_{\text{IRD}} + F_{\text{Sta}})\bar{r}. \end{aligned} \quad (4)$$

M_{R1} , M_{IRD} and M_{Sta} are the circumferential torque moment occurring from rotor 1, IRD atoms and the other atoms on stators, respectively. r_{R2} is the radius of rotor 2, \bar{r} is the average value of the radii of rotor 2 and the stator. F_{R1} is the

circumferential force on rotor 2 provided by the rotor 1, i.e.

$$F_{\text{R1}} = \frac{M_{\text{R1}}}{r_{\text{R2}}} = \sum_i -\partial P / \partial r_{ij} \cdot (\mathbf{r}_0 \cdot \boldsymbol{\tau}), \quad (5)$$

where \mathbf{r}_0 is the unit vector of \mathbf{r} with length r_{ij} between atom i on rotor 2 and atom j on rotor 1. $\boldsymbol{\tau}$ is the unit vector of the circumferential direction. P is the potential of the left end of rotor 2 with a cutoff of 1.02 nm.

Owing to thermal vibration of the atoms on rotor 2, the reaction force of IRD atoms on rotor 2, labeled as F_{IRD} , can be expressed as

$$\begin{aligned} F_{\text{IRD}} &= \frac{M_{\text{IRD}}}{\bar{r}} = \sum_i d[(\mathbf{p}_t - \mathbf{p}_0)_i \cdot \boldsymbol{\tau}] / dt \\ &= \sum_i m_i \cdot d[(\mathbf{v}_t - \mathbf{v}_0)_i \cdot \boldsymbol{\tau}] / dt \end{aligned} \quad (6)$$

where $(\mathbf{p}_0)_i$ and $(\mathbf{p}_t)_i$ are, respectively, the initial and final momentum vectors of atom i on rotor 2 in a collision with an IRD atom on the stator. A collision between two atoms is defined as starting from the appearance of a repulsive force and ending with the appearance of an attractive force. Hence, more IRD atoms on the stator will provide more opportunity for collision, which means that the rotation of rotor 2 will have a higher acceleration. The magnitudes of atomic velocities, \mathbf{v}_t and \mathbf{v}_0 , mainly depend on the temperature of the system. Hence, at higher temperatures, rotor 2 will suffer from higher repulsion during collision. This also leads to higher acceleration of the rotation of rotor 2.

$F_{\text{Sta}} = M_{\text{Sta}}/\bar{r}$ is the consultant resistance on rotor 2 provided by the other atoms on the stators, which is always against the relative sliding between rotor 2 and the stators.

It can be seen from the above results that the circumferential direction of torque moment depends on the related force direction. In equation (5) and the text above, vectors F_{R1} and F_{Sta} can be considered as friction forces. F_{IRD} can also be considered as a friction force if ω_2 (with rotor 1) is higher than ω_2 (without rotor 1). For example, if vector friction force F_{Sta} is aligned with $\boldsymbol{\tau}$, the direction of vector M_{Sta} will align with that of tube axis z and the sign of scalar M_{Sta} is positive, i.e. $M_{\text{Sta}} > 0$. The rule applies also for M_{R1} and M_{IRD} . An easy way to determine the signs of the three torque moments is given here: the direction of M_{Sta} is always opposite to the rotational direction, the directions of M_{R1} and M_{IRD} are determined by comparing the magnitude of rotational frequency of ω_1 and ω_2 (with rotor 1) and ω_2 (without rotor 1). Details are given in numerical tests.

3. Results and discussion

3.1. Without rotor 1

When the system has no rotor 1, it becomes a typical thermal-driven rotary nanomotor [22], and M_{R2} can be expressed as

$$M_{\text{R2}} = M_{\text{IRD}} + M_{\text{Sta}}. \quad (7)$$

Without rotor 1, the rotation of the free rotor 2 is determined by the value of M_{IRD} and M_{Sta} . From equations (4) and (6),

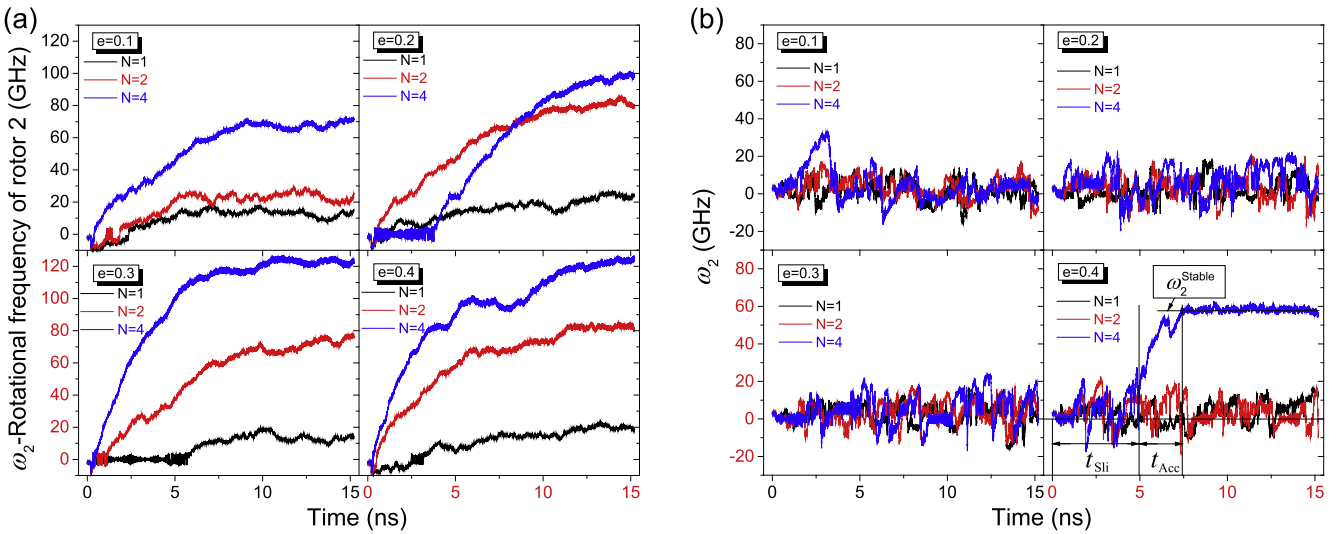


Figure 2. Rotational frequency of rotor 2 driven by stator 2 with different IRD schemes. (a) Without rotor 1 or gap 1 is much greater than 1 nm. (b) Rotor 1 has no rotation, i.e. $\omega_1 = 0$. $\omega_2 < 0$ if rotor 2 has clockwise rotation.

Table 1. The values of sliding time, acceleration time and the stable value of rotational frequency of rotor 2. The stable value is the mean value of the ω_2 in the interval [14, 15] ns. The value of sliding time is the duration from the start to the moment after which ω_2 is stably higher than 5% of the stable value of ω_2 . The acceleration time is the time between the end of sliding time to the moment when ω_2 achieves its stable value.

Sliding time (ns)								
Without rotor 1				When $\omega_1 = 0$ GHz				
	$e = 0.1$	0.2	0.3	0.4	$e = 0.1$	0.2	0.3	0.4
$N = 1$	0	0	5.51	0	15	15	15	15
$N = 2$	0	0	0.68	0	15	15	15	15
$N = 4$	0	3.60	0	0	15	15	15	4.82
Acceleration time (ns)								
$N = 1$	6.87	13.73	4.29	13.06	0	0	0	0
$N = 2$	5.57	14.28	14.32	11.32	0	0	0	0
$N = 4$	8.91	11.40	10.78	15	0	0	0	2.78
Stable value of ω_2 (GHz)								
$N = 1$	12.8	23.3	13.4	19.7	0	0	0	0
$N = 2$	20.6	82.2	74.6	82.9	0	0	0	0
$N = 4$	70.5	98.6	122.1	123.8	0	0	0	57.6

the value of M_{IRD} depends on the three factors, i.e. the temperature of system, the number of IRD atoms (N) and the relative radial deviation (e). M_{Sta} is passively determined by the relative velocity between rotor 2 and the stator and the number of atoms in their area of overlap [29, 30]. When the N IRD atoms are laid out chirally (see figure 1(b)), the final stable rotational frequency of rotor 2 will be easily obtained (see movies 1 and 2 in the supporting information). Figure 2(a) illustrates the histories of rotational frequency of rotor 2 driven by stator 2 with different IRD schemes. When M_{IRD} and M_{Sta} reach a time average equilibrium state, the stable value of ω_2 is obtained. Briefly, the magnitude of ω_2 is higher when N is higher and/or e is higher. The details are listed in table 1. Without rotor 1, the free rotor 2 can move

along the axis with a wider range. This also indicates that the acceleration process could require a longer time.

3.2. With 0 GHz rotor 1

As rotor 1 is laid out statically beside rotor 2, as shown in figure 1(a), the interaction between the two rotors has an obvious influences on the rotation of rotor 2. Figure 2(b) shows the history of ω_2 when rotor 1 has no rotation. Only when stator 2 has four IRD atoms ($N = 4$) and the relative radial deviation is 0.4 ($e = 0.4$), is rotor 2 is actuated to stable rotation, e.g. $\omega_2 = 57.6$ GHz. In movie 3, the left end of rotor 2 is attracted by the right end of rotor 1. This means that the axial oscillation of rotor 2 due to thermal vibration is limited and rotor 1 provides heavy resistance to the motion of rotor 2.

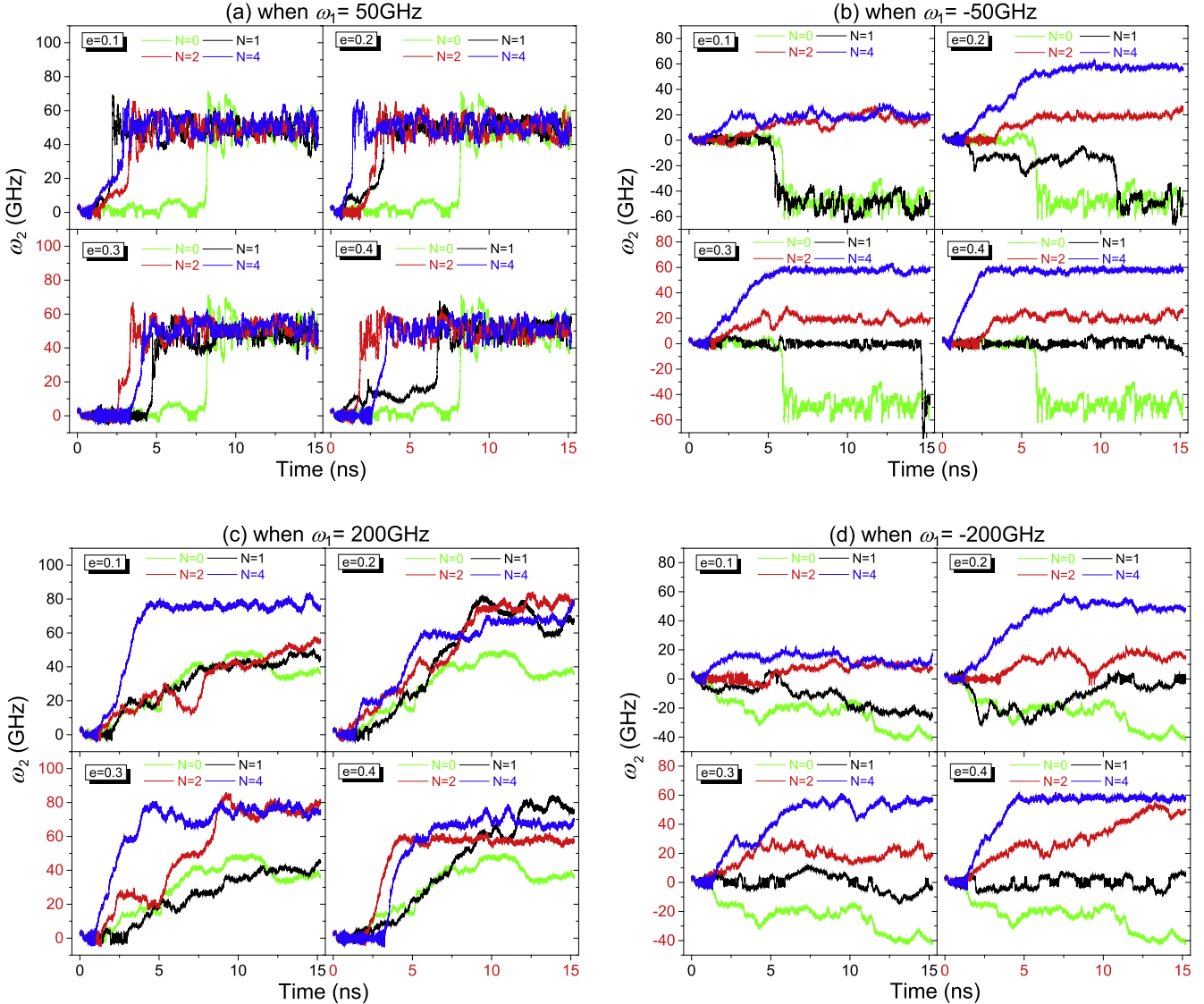


Figure 3. Rotational frequency of rotor 2 driven by stator 2 with different IRD schemes when rotor 1 has different rotational frequency.

Hence, in this condition, M_{IRD} must be higher than a threshold if the free rotor 2 can be driven to rotate.

As labeled in figure 2(b), sliding time, t_{Sli} , is the time from the start to the moment after which the rotational direction of rotor 2 remains unchanged. Acceleration time, t_{Acc} , is the time from t_{Sli} to the moment after which the rotational frequency of rotor 2 is stable. ω_2^{Stable} , the stable rotational frequency of rotor 2, occurs when the circumferential torque achieves a time average of zero. Theoretically, it can be expressed as:

$$\omega_2^{\text{Stable}}(t) = \frac{1}{2\pi} \int_{s=t_{\text{Sli}}}^{s=t_{\text{Acc}}} (M_{R2}/J_{R2}) ds, \quad M_{R2}(t \geq t_{\text{Acc}}) = 0. \quad (8)$$

3.3. With 50 GHz rotor 1

When $\omega_1 = 50\text{GHz}$, i.e. the rotational frequency of rotor 1 is 50 GHz, as shown in figure 3(a) and table 2, the final stable

value of ω_2 is nearly 50 GHz, i.e. $\omega_1 \approx \omega_2$ (with rotor 1), whatever the number of IRD atoms and the relative radial deviation of the atoms. This phenomenon indicates that the interaction between the two rotors determines the rotational state of rotor 2. Comparing the values of rotational frequency of the two rotors in the present model and the free rotor 2 (i.e. without rotor 1 standing beside it), we find that the rotational frequency of ω_2 in figure 1(a) is lower than 50 GHz, i.e. $\omega_2(\text{without rotor 1}) < \omega_2(\text{with rotor 1})$, when $N = 1$ or $N = 2$ with $e = 0.1$. This indicates that the rotation of rotor 2 is improved by the rotation of rotor 1 due to interaction between the two rotors. In this case, the value of M_{R1} is positive and the value of M_{IRD} is negative. From the rotational direction, the value of M_{Sta} is negative, too. However, when $N \geq 2$ with $e > 0.1$, the rotational frequency of the free rotor 2 is higher than 50 GHz, i.e. $\omega_2(\text{without rotor 1}) > \omega_2(\text{with rotor 1})$, which indicates that the value of M_{R1} is negative, M_{IRD} is positive and M_{Sta} is still negative (table 3). This means the

Table 2. The stable values of rotational frequency of rotor 2 in different cases (in GHz).

	When $\omega_1 = 50$ GHz				When $\omega_1 = -50$ GHz				When $\omega_1 = 200$ GHz				When $\omega_1 = -200$ GHz				
	$e = 0.1$	0.2	0.3	0.4	$e = 0.1$	0.2	0.3	0.4	$e = 0.1$	0.2	0.3	0.4	$e = 0.1$	0.2	0.3	0.4	
$N = 0$		47.0				−45.0				36.8				−37.4			
$N = 1$	44.5	48.8	48.3	53.0	−52.7	−49.5	−52.7	−2.6	46.9	65.8	40.7	77.2	−24.2	0	0	0	
$N = 2$	51.4	47.9	44.2	49.5	14.6	21.9	18.8	24.3	54.3	79.9	77.5	56.5	6.8	16.3	21.3	47.2	
$N = 4$	53.0	47.5	51.5	51.2	18.5	57.5	57.8	58.4	78.5	70.1	73.4	66.9	11.4	48.7	56.2	58.0	

Table 3. The roles of rotor 1, IRD atoms and stators in the rotational acceleration of rotor 2. (Note that if ω_2 is near 0, the influence of M_{Sta} on rotational acceleration is neglected. When w_2 is near w_1 , the influence of M_{R1} depends on M_{IRD} .)

	when $\omega_1 = 50 \text{ GHz}$	when $\omega_1 = -50 \text{ GHz}$	when $\omega_1 = 200 \text{ GHz}$	when $\omega_1 = -200 \text{ GHz}$
$N=1;$ $e=0.1$				
$N=1;$ $e=0.2, 0.3$				
$N=1;$ $e=0.4$				
$N=2;$ $e=0.1$				
$N=2;$ $e=0.2, 0.3,$ 0.4				
$N=4;$ $e=0.1, 0.3,$ 0.4				
$N=4;$ $e=0.2$				

interaction between the two rotors holds back the rotational acceleration of rotor 2.

If rotor 1 rotates clockwise, with a rotational frequency of 50 GHz (when $\omega_1 = -50 \text{ GHz}$), from figure 3(b) rotor 2 behaves differently from the situation shown in figure 3(a). For example, when $N = 0$, rotor 2 rotates synchronously with rotor 1. The rotational direction of rotor 2 is different from that of rotor 1 when $N \geq 2$. In particular, when $N = 1$, the rotational state of rotor 2 depends on the value of relative deviation (e). For instance, when $e = 0.1$, after $\sim 5 \text{ ns}$ of sliding time, the rotation of rotor 2 is actuated successfully. The two rotors rotate synchronously. If $e = 0.2$, the rotation of rotor 2 needs a long acceleration time to approach the stable value. If $e = 0.3$, the sliding time becomes longer, e.g. $\sim 14.4 \text{ ns}$. If $e = 0.4$, the rotation of rotor 2 is not actuated within 15 ns . Clearly, for a model with the same value of N , a

higher value of e (in the interval $[0.1, 0.4]$) means that a higher value of M_{IRD} is applied on rotor 2, and clockwise rotation of rotor 2 will be held back more strongly. Until $N = 2$, and $e > 0.1$, rotor 2 rotates inversely to rotor 1. These results also suggest a way to find the threshold of M_{IRD} .

3.4. With 200 GHz rotor 1

To gain a deep understanding of the influence of the relative velocity between the two rotors on the dynamic response of rotor 2, we also provide the histories of ω_2 when the 200 GHz rotor 1 rotates either anti-clockwise (figure 3(c)) or clockwise (figure 3(d)).

For $\omega_2 = 200 \text{ GHz}$, when $N = 0$, the stable value of rotational frequency of rotor 2 driven by rotor 1 is $\sim 36.8 \text{ GHz}$. This is because rotor 2 can oscillate along its axis freely during rotation if there is no IRD atom at the end of

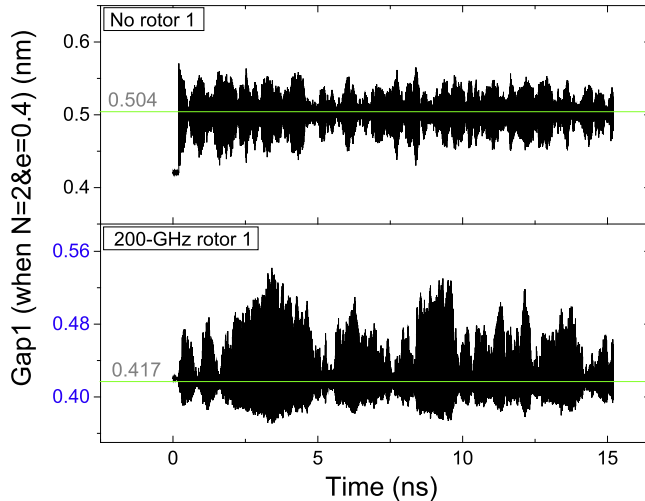


Figure 4. Mass center history of rotor 2 in a motor with $N = 2$, $e = 0.4$. When the system does not have a rotor 1, the equivalent value of gap 1 varies around 0.504 nm and the history curve is approximately symmetric along the green line. If the system has a 200 GHz rotor 1, gap 1 fluctuates around 0.417 nm. The curve below the green line has smaller amplitude than that above the green line, which indicates that rotor 2 is subjected to stronger repulsion from rotor 1 and weaker repulsion from stator 1.

stator 2. The interaction between the two rotors is reduced, which means that a lower stable rotational frequency can be actuated. When $N = 1$, without disturbance from rotor 1, the rotational frequency of rotor 2, i.e. ω_2 (without rotor 1), will be in the interval [10, 25] GHz as $e \in [0.1, 0.4]$ (figure 2(a)). With a 200 GHz rotor 1, ω_2 (with rotor 1) will be in the interval [40, 80] GHz (figure 3(c)). Hence, the stable value of ω_2 is improved by adding rotor 1 when $N > 0$. In this condition, M_{IRD} and M_{Sta} provide negative acceleration on the rotation of rotor 2 (table 3). When $N = 2$ and $e = 0.1$, ω_2 is ~ 20.6 GHz (without rotor 1) or ~ 54.3 GHz (with 200 GHz rotor 1). M_{IRD} and M_{Sta} provide negative acceleration on the rotation of rotor 2, too. When $N = 2$ and $e = 0.2$ or 0.3 , the stable value of ω_2 (without rotor 1) will be very close to that of rotor 2 driven by rotor 1 at 200 GHz. In these cases, M_{IRD} should fluctuate around zero. When $N = 2$ and $e = 0.4$, the stable value of ω_2 (without rotor 1) is ~ 82.9 GHz (figure 2(a)). However, the stable value is only ~ 56.5 GHz when rotor 2 is driven by rotor 1 at 200 GHz. This means that the rotational frequency of rotor 2 is reduced rather than improved by the interaction between the two rotors. Similarly, we also find this phenomenon when $N = 4$ and $e > 0.1$. The mechanism can be revealed easily, namely, rotor 2 is attracted by rotor 1 at its left end, whilst it is driven by the IRD atoms at its right end. The axial oscillation of rotor 2 is limited by the existence of both IRD atoms and rotor 1 (figure 4). And the collision between the atoms on rotor 2 and the IRD atoms on stator 2 is reduced along the circumferential direction. Meanwhile, the IRD atoms provide positive acceleration for rotation of rotor 2. Hence, the final stable rotational frequency of rotor 2 driven by a high-speed rotor 1 may be lower than that of a free rotor 2.

When $\omega_1 = -200$ GHz, i.e. rotor 1 rotates clockwise with a frequency of 200 GHz, rotor 2 rotates differently from rotor 1. For example, from figure 3(d), no stable value of ω_2 in any case is near -200 GHz. Briefly, the rotational directions of the two rotors are the same if $N = 0$ or $N = 1$ with $e = 0.1$. As a time average, the value of ω_2 is near zero if $N = 1$ with $e > 0.1$. If $N = 2$ or 4 and e is in the interval $[0.1, 0.4]$, rotor 2 rotates anti-clockwise, and the rotational frequency is in the interval $[0, 60]$ GHz (table 2). This range is identical to that of rotor 2 driven by a -50 GHz rotor 1.

4. Conclusions

In nanodevices with rotary components, the rotational state of the components may need adjustment to meet the particular requirements. In nanoscale, the interaction between two items will be strong enough to influence their dynamic response when the distance between them is less than 1 nm. In investigating the end interfacial interaction between two rotary nanotubes with the same chirality, some typical numerical examples are tested, and the following conclusions can be drawn.

- (1) Without rotor 1, the free rotor 2 can be actuated to rotate easily if the stators have one or more IRD atoms at the end. If rotor 1 stands statically beside rotor 2, rotor 2 can be driven to rotate only when the circumferential torque moment provided by the IRD atoms is higher than a threshold. Increasing the number of IRD atoms and the relative radial deviation can improve the torque moment to exceed the threshold. This also suggests potential application of a nanoengine/governor/brake in such rotary system.
- (2) When the two rotors have the same rotational direction, rotor 2 will rotate synchronously with rotor 1 which has lower rotational frequency, e.g. 50 GHz in present model, than the stable rotational frequency of the free rotor 2.
- (3) If the stator has no IRD atom, and the two rotors have the same rotational direction, rotor 2 driven by the high-speed rotor 1 rotates more slowly than the free rotor 2. The reason is that without the IRD atoms, rotor 2 can oscillate freely along its axis, which leads to a decreasing interaction between the two rotors.
- (4) When the stator has higher number of IRD atoms with higher relative radial deviation, and the two rotors rotate along the same direction, the stable rotational frequency of rotor 2 will be reduced to a lower value than that of the system with a free rotor 2. The reason is that the axial oscillation of rotor 2 is confined by the IRD atoms during rotation.
- (5) Comparing the difference in rotation of rotor 2 driven by rotor 1 with different speeds of rotation, a higher relative rotational speed between the two rotors will provide lower friction on rotor 1, which is opposite to

that between neighboring shells in MWCNTs. This will be useful for designing a nanoengine governor.

References

- [1] Iijima S 1991 Helical microtubules of graphitic carbon *Nature* **354** 56–8
- [2] Rueckes T, Kim K, Joselevich E, Tseng G Y, Cheung C-L and Lieber C M 2000 Carbon nanotube-based nonvolatile random access memory for molecular computing *Science* **289** 94–7
- [3] Peng H, Chang C, Aloni S, Yuzvinsky T and Zettl A 2006 Ultrahigh frequency nanotube resonators *Phys. Rev. Lett.* **97** 087203
- [4] Garcia-Sanchez D, San Paulo A, Esplandiu M J, Perez-Murano F, Forró L, Aguasca A and Bachtold A 2007 Mechanical detection of carbon nanotube resonator vibrations *Phys. Rev. Lett.* **99** 085501
- [5] Lassagne B, Tarakanov Y, Kinaret J, Garcia-Sanchez D and Bachtold A 2009 Coupling mechanics to charge transport in carbon nanotube mechanical resonators *Science* **325** 1107–10
- [6] Cumings J and Zettl A 2000 Low-friction nanoscale linear bearing realized from multiwall carbon nanotubes *Science* **289** 602–4
- [7] Zheng Q and Jiang Q 2002 Multiwalled carbon nanotubes as gigahertz oscillators *Phys. Rev. Lett.* **88** 045503
- [8] Legoa S, Coluci V, Braga S, Coura P, Dantas S and Galvao D 2003 Molecular-dynamics simulations of carbon nanotubes as gigahertz oscillators *Phys. Rev. Lett.* **90** 055504
- [9] Sazonova V, Yaish Y, Üstünel H, Roundy D, Arias T A and McEuen P L 2004 A tunable carbon nanotube electromechanical oscillator *Nature* **431** 284–7
- [10] Cai K, Yin H, Qin Q H and Li Y 2014 Self-excited oscillation of rotating double-walled carbon nanotubes *Nano Lett.* **14** 2558–62
- [11] Qiu W, Kang Y, Lei Z K, Qin Q H and Li Q 2009 A new theoretical model of a carbon nanotube strain sensor *Chin. Phys. Lett.* **26** 080701
- [12] Qiu W, Kang Y L, Lei Z K, Qin Q H, Li Q and Wang Q 2010 Experimental study of the Raman strain rosette based on the carbon nanotube strain sensor *J. Raman Spectrosc.* **41** 1216–20
- [13] Qiu W, Li Q, Lei Z K, Qin Q H, Deng W L and Kang Y L 2013 The use of a carbon nanotube sensor for measuring strain by micro-Raman spectroscopy *Carbon* **53** 161–8
- [14] Fennimore A, Yuzvinsky T, Han W-Q, Fuhrer M, Cumings J and Zettl A 2003 Rotational actuators based on carbon nanotubes *Nature* **424** 408–10
- [15] Bourlon B, Glattli D C, Miko C, Forró L and Bachtold A 2004 Carbon nanotube based bearing for rotational motions *Nano Lett.* **4** 709–12
- [16] Kang J W and Hwang H J 2004 Nanoscale carbon nanotube motor schematics and simulations for micro-electro-mechanical machines *Nanotechnology* **15** 1633
- [17] Tu Z and Hu X 2005 Molecular motor constructed from a double-walled carbon nanotube driven by axially varying voltage *Phys. Rev. B* **72** 033404
- [18] Barreiro A, Rurali R, Hernandez E R, Moser J, Pichler T, Forró L and Bachtold A 2008 Subnanometer motion of cargoes driven by thermal gradients along carbon nanotubes *Science* **320** 775–8
- [19] Hamdi M, Subramanian A, Dong L, Ferreira A and Nelson B J 2013 Simulation of rotary motion generated by head-to-head carbon nanotube shuttles *IEEE/ASME Trans. Mechatronics* **18** 130–7
- [20] Cai K, Li Y, Qin Q H and Yin H 2014 Gradientless temperature-driven rotating motor from a double-walled carbon nanotube *Nanotechnology* **25** 505701
- [21] Cai K, Yu J, Yin H and Qin Q H 2015 Sudden stoppage of rotor in a thermally driven rotary motor made from double-walled carbon nanotubes *Nanotechnology* **26** 095702
- [22] Cai K, Wan J, Qin Q H and Shi J 2016 Quantitative control of a rotary carbon nanotube motor under temperature stimulus *Nanotechnology* **27** 055706
- [23] Cai K, Yu J, Shi J and Qin Q 2015 A method for measuring rotation of a thermal carbon nanomotor using centrifugal effect *Sci. Rep.* **6** 27338
- [24] Collins P G and Avouris P 2000 Nanotubes for Electronics *Sci. Am.* **283** 62–70
- [25] Qin Z, Qin Q-H and Feng X-Q 2008 Mechanical property of carbon nanotubes with intramolecular junctions: molecular dynamics simulations *Phys. Lett. A* **372** 6661–6
- [26] Zhang R, Ning Z, Zhang Y, Zheng Q, Chen Q, Xie H, Zhang Q, Qian W and Wei F 2013 Superlubricity in centimetres-long double-walled carbon nanotubes under ambient conditions *Nat. Nanotechnol.* **8** 912–6
- [27] Servantir J and Gaspard P 2006 Rotational dynamics and friction in double-walled carbon nanotubes *Phys. Rev. Lett.* **97** 186106
- [28] Kis A, Jensen K, Aloni S, Mickelson W and Zettl A 2006 Interlayer forces and ultralow sliding friction in multiwalled carbon nanotubes *Phys. Rev. Lett.* **97** 025501
- [29] Zhu C, Guo W and Yu T 2008 Energy dissipation of high-speed nanobearings from double-walled carbon nanotubes *Nanotechnology* **19** 465703
- [30] Guo Z, Chang T, Guo X and Gao H 2011 Thermal-induced edge barriers and forces in interlayer interaction of concentric carbon nanotubes *Phys. Rev. Lett.* **107** 105502
- [31] Cook E H, Buehler M J and Spakovszky Z S 2013 Mechanism of friction in rotating carbon nanotube bearings *J. Mech. Phys. Solids* **61** 652–73
- [32] Cai K, Yin H, Wei N, Chen Z and Shi J 2015 A stable high-speed rotational transmission system based on nanotubes *Appl. Phys. Lett.* **106** 021909
- [33] Yin H, Cai K, Wan J, Gao Z and Chen Z 2016 Dynamic response of a carbon nanotube-based rotary nano device with different carbon–hydrogen bonding layout *Appl. Surf. Sci.* **365** 352–6
- [34] Cai K, Cai H, Ren L, Shi J and Qin Q-H 2016 Over-speeding rotational transmission of a carbon nanotube-based bearing *J. Phys. Chem. C* **120** 5797–803
- [35] 2016 LAMMPS, Molecular dynamics simulator. (<http://lammps.sandia.gov/>)
- [36] Plimpton S 1995 Fast parallel algorithms for short-range molecular dynamics *J. Comput. Phys.* **117** 1–19
- [37] Stuart S J, Tutein A B and Harrison J A 2000 A reactive potential for hydrocarbons with intermolecular interactions *J. Chem. Phys.* **112** 6472–86
- [38] Jones J E 1924 On the determination of molecular fields: II. From the equation of state of a gas *Proc. R. Soc., A* **106**, 463–77.